Ferri, O.M.; Ebel, T.; Bormann, R.:

The Influence of a Small Boron Addition on the Microstructure and Mechanical Properties of Ti-6Al-4V Fabricated by Metal Injection Moulding

In: Advanced Engineering Materials (2011) Wiley

DOI: 10.1002/adem.201000280

The influence of a small boron addition on the microstructure and mechanical properties of Ti-6Al-4V fabricated by metal injection moulding

Authors: O.M. Ferri, T. Ebel, R. Bormann

Affiliation: GKSS Research Centre, Institute of Materials Research, Max-Planck-Str. 1, D-21502 Geesthacht, Germany

Abstract

The effect of boron additions on the sintering behaviour, microstructural development and mechanical properties of a Ti-6Al-4V alloy fabricated by metal injection moulding (MIM) was studied. The addition of boron promotes a significant refinement of the microstructure by changing the microstructure from the typical lamellar to a more equiaxed morphology. The presence of both features: α colonies and α grains was confirmed by electron backscatter diffraction (EBSD) experiments. Furthermore, the pinning effect of TiB particles on grain boundary motion enhances the densification process due to the fact that the separation of pores and grain boundaries is suppressed. As a result of the refinement of the microstructure achieved by adding 0.5 wt. % boron to the Ti-6Al-4V alloy, excellent tensile ($\sigma_{0.2}$ = 787 MPa, UTS = 902 MPa and ε = 12%) and fatigue (endurance limit = 640 MPa) properties were obtained.

Key words: metal injection moulding (MIM); sintering; titanium alloys; microstructure; fatigue

1. Introduction

During the last few years, there has been a remarkable increase in research on conventional titanium alloys containing small additions of boron, mainly due to the microstructure refinement promoted by boron additions [1-6]. Bermingham et al. [3] and Tamirisakandala et al. [4] suggested that grain refinement occurs via a solute mechanism and growth restriction theory. Furthermore, Komizo et al. [7] demonstrated by using high-temperature laser scanning confocal microscopy that TiB particles act as heterogeneous nucleation sites for the α titanium phase and as barriers to β grain growth at high temperatures. In situ TiB whiskers/particles are particularly attractive for titanium alloys since the TiB phase has not only a high modulus, but also approximately the same coefficient of thermal expansion as the matrix as well as chemical compatibility. Several processing techniques have been developed in recent decades in order to optimise the structure and properties of in situ ceramic phase reinforced materials [8]. Powder metallurgy, more specifically Metal Injection Moulding (MIM), is a net-shape process that can be applied in order to obtain a discontinuously reinforced material with a homogeneous microstructure at relatively low cost [9]. Currently, it is possible to fabricate Ti-6Al-4V alloy components by MIM with excellent tensile properties (UTS > 800 MPa, ε > 14%) [10]. However, components such as permanent implants, automotive parts and some special aerospace parts are required to have extremely high reliability, especially under fatigue conditions. Unfortunately, the performance of MIM components with respect to fatigue resistance is generally not as good as demonstrated for the tensile behaviour. Recent investigations on Ti-6Al-4V [11, 12] have shown that the fatigue endurance limit at 10^7 cycles is in the range 350 to

400 MPa. This value is significantly lower than the endurance limit of ~ 600 MPa for wrought material after annealing to give a fully lamellar microstructure [13]. It is also much lower than the endurance limit of ~ 800 MPa obtained for the thermo-mechanically treated Ti-6Al-4V alloy with an equiaxed microstructure [14]. However, other recent investigations have shown that it is possible to increase the fatigue resistance of Ti-6Al-4V components produced by MIM technology by changing the surface quality [15] or by controlling specific processing parameters such as binder content [16] and powder particle size [11]. Nevertheless, better fatigue resistance is still desirable for MIM parts. One possibility to further increase the fatigue strength is the refinement of the microstructure and as discussed before the addition of boron can promote such an effect in the Ti-6Al-4V alloy.

Surprisingly, no systematic work has been performed to date in order to relate the effect of boron additions in Ti-6Al-4V alloy components produced by MIM. This paper aims to clarify the influence of boron additions on the sintering behaviour, microstructure and mechanical properties of Ti-6Al-4V fabricated by the MIM technique.

2. Experimental

2.1 Materials and processing

The materials used in this work were gas atomised, spherical, Ti-6Al-4V ELI (ASTM grade 23) alloy powder supplied by TLS Technik GmbH, Germany, with a particle size < 45 µm and amorphous boron powder (grade I, 95% purity) supplied by H.C. Starck, Germany, with a particle size < 2 µm. The addition of 0.5 wt. % amorphous boron powder was carried out during feedstock preparation. Two feedstocks (mixtures of the

powders and the binder system) with and without amorphous boron powder were prepared. The feedstock contained 35 vol. % of binder system (polyethylene, paraffin and stearic acid). The feedstock was prepared and mixed in a Z-blade mixer at a temperature of 120 °C for two hours under an argon atmosphere. Two different specimen geometries were moulded: cuboids (48.8 mm x 3.3 mm x 6.1 mm) for bending fatigue experiments and standard "dog-bone" tensile test samples of length 89 mm and diameter 5 mm. A maximum pressure of 950 bar at an injection rate of 20 cm^3/s and a maximum cylinder temperature of 120 °C were used during the injection process.

After moulding, the samples were immersed in heptane at 40 °C for 20 h in order to remove the paraffin. Thermal debinding of the remaining binder and subsequent sintering was performed in a single-step heat treatment. Sintering was carried out in a vacuum of 10^{-5} mbar at temperatures of 1250 °C and 1400 °C for two hours followed by controlled furnace cooling at 10 °C/min.

It is well known that a small addition (~ 0.1 wt.%) of boron to cast Ti-6Al-4V decreases the as-cast grain size by approximately one order of magnitude [4]. However, such an effect may not occur during the sintering process. Therefore, MIM Ti-6Al-4V alloy samples with and without 0.5 wt. % boron were sintered in order to evaluate the changes in the microstructure.

2.2 Characterization of the samples

The influence of boron addition on the sintering behaviour of Ti-6Al-4V was studied by dilatometry. For this experiment, MIM samples (diameter 5 mm, length 10 mm) of Ti-6Al-4V and Ti-6Al-4V-0.5B were chemically and thermally debound followed by pre-sintering at 700 °C for 60 min. The dilatometer used was a vertical configuration dilatometer fabricated by LINSEIS (L70/2171). An initial pressure of 150 mN was applied before starting the experiment. A heating rate of 10 °C/min and an isothermal treatment of two hours at 1400 °C were used. An argon atmosphere was applied during the heating and cooling processes.

Electron backscatter diffraction (EBSD) was performed on a ZEISS (ULTRA^{TM} 55) scanning electron microscope equipped with a Hikari camera and TSL OIM Analysis 5.2 software. Spatially resolved EBSD maps were acquired at 15 keV using a step size of 0.2 µm. The samples were prepared by conventional polishing procedures followed by final polishing (5 min) with a Struers oxide polish suspension (OPS) compound. When electropolishing $\alpha + \beta$ titanium alloys, the β phase is attacked preferentially. This makes it impossible to detect the β phase and its texture during EBSD mapping. For this reason, the samples were finally polished in a vibratory machine (Buehler Vibromet 2) for 48 hours in a colloidal silica suspension (MasterMet$^{®}$ 0.06 µm).

Electron backscatter diffraction patterns (EBSPs) were used in order to clarify the crystallographic structure of the boride phase. The lattice parameters and the fractional coordinates of atoms in TiB and TIB_2 are given in Table 1 [17].

Optical microscopy was used in order to investigate the microstructures. The average α colony size in the Ti-6Al-4V alloy samples was measured using an image analysis system (Olympus Soft Image Solution, analysis pro). For the samples with boron, the grain size was estimated from EBSD images. A linear intercept technique (ASTM E112-96) was applied in order to determine the grain size. The impurity levels were determined for samples sintered at 1400 °C by using a conventional LECO melt extraction system. The TC-436AR equipment was used to analyse the nitrogen and oxygen levels. The CS-444 was applied in order to determine the carbon content. The relative density of sintered samples was determined by the immersion method outlined in ASTM B311. The bulk density of Ti-6Al-4V alloy without pores was estimated to be 4.41 g/cm^3 after measuring a sample exposed to an additional hot isostatic pressing (HIP) process following MIM processing. Therefore, it was possible to estimate the porosity of the sintered samples with the following equation:

$$\text{Relative densification}\,[\%] = \left[\left(\frac{\rho_S}{\rho_0}\right) \bullet 100\right] \qquad \textbf{1}$$

Where ρ_s is the apparent sintered density measured by the immersion method and ρ_0 is the bulk density of the Ti-6Al-4V alloy component without pores.

Tensile tests on three Ti-6Al-4V-0.5B specimens sintered at 1400 °C were performed on a servohydraulic structural test machine equipped with a 100 kN load cell. The tensile tests were carried out at room temperature at a strain rate of 1.2 x 10^{-5} s^{-1}.

The results of the tensile and fatigue tests on Ti-6Al-4V-0.5B sintered at 1400 °C were compared to those measured in a previous investigation [15]. The four-point bending

fatigue tests were carried out on the samples with 0.5 wt. % boron sintered at 1400 °C. Before fatigue testing, all samples were shot peened in order to obtain approximately the same surface quality. The shot peening was performed with an air-blast machine using fine zirconium oxide particles with a diameter of 500 µm. The exposure time for each surface was 10 s and the air pressure used was 4 bar. The working distance was 50 mm and the nozzle diameter used was 6 mm.

High cycle fatigue testing was carried out in a four-point bending configuration using a resonance machine fabricated by RUMUL (Mikrotron 654-H, 20kN). Tests were conducted under load control with a cyclic frequency of ~ 95 Hz (sine wave) and a load ratio $R=\sigma_{min}/\sigma_{max}$ of 0.2. All the experiments were carried out at room temperature in air. The fatigue endurance limit was defined as 10^7 cycles.

The maximum initial tensile stress σ within the loaded bar was calculated using equation 2 where F is the applied force, L is the gauge length, W is the bar thickness and $(I_{xx})_r$ is the moment of inertia of rectangular cross section with corner radius r.

$$\sigma = \frac{FLW}{24(I_{xx})_r} \qquad \textbf{2}$$

The true moment of inertia $(I_{xx})_r$ about the neutral axis x-x is:

$$(I_{xx})_r = \frac{B(W-2r)^3}{12} + \frac{(B-2r)r^3}{6} + (1/2)(B-2r)(W-r)^2 r + 4r^4\left(\frac{\pi}{16} - \frac{4}{9\pi}\right) + \pi r^2\left[\frac{W}{2} - r\left(1 - \frac{4}{3\pi}\right)\right]^2 \qquad \textbf{3}$$

where B is the bar width and r is the corner radius.

The fracture surfaces of the samples were investigated using a scanning electron microscope (ZEISS – DSM962). The observations were focused on locating the crack initiation sites. In an effort to understand the influence of the microstructural features on fatigue crack nucleation and propagation, crack front profiles at the possible crack nucleation sites were investigated.

3. Results

3.1. Influence of boron addition on the microstructure

Table 2 shows the amount of interstitial elements for samples with and without boron addition. Similar values were obtained in both cases. As can be seen in Figs. 1 and 2, the addition of boron significantly modifies a number of microstructural features. The samples without boron addition exhibit a fully lamellar microstructure with alternating α and β phases having a distinct orientation relationship (α colony). The samples with boron exhibit a microstructure with α colonies and single α grains, which resembles a quasi-equiaxed microstructure. Residual porosity is present in all samples investigated.

In this investigation, the grain size was assumed to be the microstructural feature that defines the slip length. Therefore, the α colony size (Fig. 1a , length (I)) and α phase (Fig. 2b, length (II)) or α colony (Fig. 2b, length (I)) sizes are the features that define a grain for lamellar and quasi-equiaxed microstructure, respectively. In terms of α colony size in the Ti-6Al-4V alloy, samples with no addition of boron showed mean values of α colonies of approximately 77 ± 9 µm and 247 ± 22 µm for samples sintered at 1250 °C and 1400 °C, respectively. The relative density increases from approximately 96.5 % for samples sintered at 1250 °C to 97 % for samples sintered at 1400 °C.

Due to difficulties defining the grain boundaries of the samples with the boron addition by means of light microscopy, the EBSD technique was applied in order to estimate the grain size. The results are presented in section 3.3. The addition of 0.5 wt. % of boron significantly decreases the relative densification to a value of approximately 91 % for samples sintered at 1250 °C. On the other hand, samples containing boron sintered at 1400 °C achieved a relative densification of 98 %. This is a clear indication that the formation of TiB particles (the particles in the form of needles marked by the white arrows in Figs. 2a and b) affects the sintering behaviour of the Ti-6Al-4V alloy. Therefore, a better understanding of the sintering process of the Ti-6Al-4V alloy powder with additions of amorphous boron powder is required. One technique that is very helpful in describing the evolution of the sintering process is dilatometry.

3.2. - Dilatometry

Fig. 3a and b illustrate the linear shrinkage (LS) and the linear shrinkage rate (LSR) of the Ti-6Al-4V alloy with and without 0.5 wt. % boron, respectively. The Ti-6Al-4V alloy started to shrink earlier compared to the samples with the boron addition. Above 820 °C, the Ti-6Al-4V-0.5B sample exhibited a significant decrease in the LSR up to approximately 1048 °C. The Ti-6Al-4V alloy exhibited a maximum LSR of 0.27 %/min at approximately 985 °C. Above this temperature the LSR started to decrease. On the other hand, the Ti-6Al-4V-0.5B alloy started to shrink significantly above 1048 °C. The maximum LSR achieved in this alloy during dilatometry experiments was ~ 0.45 %/min at approximately 1252 °C. The maximum LSR obtained for Ti-6Al-4V-0.5B was approximately two times higher. Additionally, the alloys with and without boron

exhibited an LS after two hours at 1400 °C of approximately 13.6 % and 12.9 %, respectively. It is important to note that the LS of the Ti-6Al-4V-0.5B alloy reached higher values than the Ti-6Al-4V alloy only after 33 minutes at 1400 °C, although it started later.

3.3. Grain size and phase distribution

Using EBSD measurements (Fig. 4) it was possible to identify clearly the phases and the orientation of these phases in the Ti-6Al-4V-0.5B sample sintered at 1400 °C. Each different colour represents a different orientation. Regions with α colonies (α lamellae with the same orientation) and a single α grain (no β phase was detected in these specifics grains, which is a typical characteristic of the equiaxed microstructure) were observed in Fig. 4b. Furthermore, it was possible to clearly identify the β phase (Fig. 4c) and the related orientations. Information regarding the prior β phase grain size was obtained by analysing the β phase regions with the same orientation. Two more phases were investigated during the EBSD measurements: TiB and TiB_2. However, only the TiB phase (Fig. 4d) was indexed and no TiB_2 particles were identified.

The average grain size (α colonies and α grains) measured is 18 ± 5 μm which is a significant reduction compared to the 247 ± 22 μm α colony size measured for Ti-6Al-4V alloy sintered at 1400 °C.

A higher magnification was used in order to better identify these two regions (α colonies and α grains). The regions defined as (I) in Fig. 5b refer to the α colonies. Note that only few lamellae have the same orientation (same colour) in a specific α colony.

The regions (II) indicate a single α grain with no orientation relationship to the neighbouring α phase lamellae or grain.

In order to provide more evidence of the influence of the boron addition on the microstructural changes, a pure MIM Ti-6Al-4V sample sintered at 1400 °C was also subjected to EBSD analysis, (Fig. 6). As illustrated in Fig. 6b the α colonies are significantly larger than in the samples containing boron (Fig. 4b). Furthermore, a comparison between Figs. 6a and c illustrates that not all of the rather thin β regions (white phase in Fig. 6a) could be indexed properly by the EBSD analysis. Nevertheless, it is clear that the mean size of the β phase regions with the same orientation (same colour) in the sample with boron (Fig. 4c) is much smaller than that of the pure Ti-6Al-4V sample (Fig. 6c).

3.4. Mechanical Behaviour

The tensile and fatigue properties of the Ti-6Al-4V-0.5B samples sintered at 1400 °C will be compared to previous results obtained on Ti-6Al-4V samples sintered at 1250 °C as reference values.

3.4.1. Tensile behaviour

The alloy containing 0.5 wt. % boron exhibits very attractive tensile properties. Table 3 illustrates the mechanical properties of the alloys with and without the boron addition. A significant increase in yield strength and UTS is observed for the alloy with boron. On the other hand, the elongation to failure decreases by approximately 2 % with the presence of boron.

The white arrows in Fig. 7 indicate broken TiB particles and interfacial decohesion between TiB particles and the matrix. Moreover, fine and coarse dimples with residual porosity are typical features of the tensile fracture surface of Ti-6Al-4V-0.5B samples.

3.4.2. Fatigue behaviour

The four-point bending fatigue life response of the Ti-6Al-4V and Ti-6Al-4V-0.5B alloys processed by MIM is shown in Fig. 8. The addition of boron promoted a significant increase in the fatigue resistance. The endurance limit was approximately 640 MPa.

Fig. 9 shows an overview of a typical fracture surface of the Ti-6Al-4V-0.5B samples, indicating that the crack initiated in some place near the lower right corner. The apparent nucleation site is located inside the sample instead of at the surface. As can be seen in Fig. 10, quasi-cleavage facets and pores were observed in the possible crack nucleation location. Another interesting aspect of the crack nucleation location is evidence of a possible interfacial decohesion (pull-out) between TiB particles and the matrix as pointed out by the white arrow in Fig. 10.

The black line in Fig. 9 illustrates approximately the region where the crack front profile (Fig. 11) was situated. The left side of Fig. 11 represents the lower right corner of Fig. 9, which is the assumed crack initiation site. Flat surfaces (indication of quasi-cleavage fracture) and secondary cracks are typical features of the crack front profile

near the assumed crack nucleation site. These features are not present on the right side of the crack front profile.

Fig. 12 illustrates clearly the interfacial decohesion between the matrix and the TiB particles. Apparently, the crack propagated around the particles and no evidence of an eventual particle fracture was observed during the investigation at the assumed crack nucleation regions.

4 Discussion

4.1. Microstructure morphology

As expected and reported before for several sintered materials [18] including the Ti-6Al-4V alloy [10] coarsening of the microstructure (Figs. 1a and b) is observed in Ti-6Al-4V samples sintered at higher temperatures. This process is enhanced within the single phase β region which facilitates fast grain growth, whereas the α phase which could act as a growth barrier is first formed during cooling.

For the Ti-6Al-4V-0.5B samples (see Fig. 2) the α colony size is not well defined which can be related to a tendency to form equiaxed α instead of the lamellar structure. Such behaviour was also reported in the work of Hill et al. [19] for a cast Ti-6Al-4V alloy with a small addition of boron. They obtained the equiaxed microstructure after an additional heat treatment with slow cooling from above the β transus without any thermo-mechanical treatment in the α + β phase field (a typical procedure to create globular microstructures in α + β titanium alloys). They suggested that α nucleating at

and growing from the TiB precipitates usually results in an equiaxed or globular morphology.

Tamirisakandala et al. [4] also tried to describe the mechanism responsible for the microstructural refinement in the cast Ti-6Al-4V with small additions of boron. In their study, the refinement of the microstructure was explained by three mechanisms: refinement of prior β-grains, heterogeneous α nucleation and grain growth restriction. The prior β-grain refinement was related to the influence of boron partitioning ahead of the titanium solid/liquid interface. More recently, Bermingham et al. [3] described similar observations for cast commercially pure titanium with a small addition of boron. The second mechanism, heterogeneous α nucleation, is related to the influence of TiB particles on the nucleation of the α phase. They suggested that the presence of TiB particles enhanced the kinetics of phase transformation from β to α, which occurs by nucleation and growth according to the Burger's orientation relationship, by providing additional nucleation sites. A microstructure with equiaxed α grains is more likely to occur as a consequence of these additional nucleation sites. Finally, the grain growth restriction mechanism is related to the pinning effect promoted by the TiB particles on grain growth. In cast materials, this mechanism is assumed to be relevant during subsequent thermal exposure at elevated temperatures by restricting the mobility of grain boundaries.

It is important to note that the mechanism for refinement of the prior β-grains is not likely to occur in the sintered MIM Ti-6Al-4V-0.5B samples since no liquid phase is expected to be present during the sintering process. However, as for the cast Ti-6Al-4V

alloy with a small addition of boron, heterogeneous α nucleation at TiB particles is a relevant mechanism in order to describe the microstructural changes in the MIM Ti-6Al-4V-0.5B samples after sintering. Although the grain growth restriction is assumed to be a secondary microstructural refinement mechanism for the cast Ti-6Al-4V alloy with a small addition of boron, this mechanism is relevant for the sintering process and for the final microstructure of the MIM samples (see section 4.2).

In the Ti-6Al-4V-0.5B alloy, both α colonies and α grains were assumed to define the grain size (slip length) because both features co-exist in the microstructure. Fig 5b shows regions (I) where α lamellae are oriented in the same direction, setting up a colony. However, regions (regions II) can also be observed where neighbouring single α phases have no correlated orientation. The microstructure of the samples with 0.5 wt. % boron cannot be considered as typically lamellar with well defined α colonies. In fact, the sintered microstructure can be considered as a transition between lamellar and equiaxed microstructures (see Fig. 2, Fig. 4 and Fig. 5).

In addition, it was possible to clearly identify the β phase between these α lamellae and at the grains boundaries (Fig. 4c). The prior β grain size of the samples with the boron addition is apparently smaller than that of the samples without boron (Fig. 6c). This is an indication that the TiB particles act as a barrier to grain growth of prior β grains during sintering.

Three boron compounds exist in the Ti-B system: TiB, Ti_3B_4 and TiB_2. Feng et al. [20] stated that only TiB can be synthesized in situ from the reaction between Ti powder and

boron powder. In this investigation, only the TiB phase (Fig. 4d) was indexed during the EBSD experiments and no TiB_2 was observed in the Ti-6Al-4V-0.5B alloy. This is in agreement with thermodynamic expectations [17, 21-24] and with the Feng et al. [20] statement.

Another interesting aspect of the Ti-6Al-4V-0.5B alloy microstructure produced by MIM technology is the apparent homogeneous distribution of the TiB particles. This is a clear advantage of the MIM process over the casting process. As reported by Srinivasan et al. [25], the cast Ti-6Al-4V alloy with a small addition of boron (0.1 wt.%) tends to exhibit a microstructure with TiB precipitated at the grain boundaries. This preferential precipitation at the grain boundaries promotes degradation in the mechanical properties, especially with respect to the tensile elongation to failure.

4.2 The sintering process

The addition of boron to Ti-6Al-4V delays the start temperature of the shrinkage process by almost 100 °C as illustrated in Fig. 3. As stated by German [26], the shrinkage of the powder compact is a result of a change in the interparticle spacing as neck growth takes place which is promoted by bulk transport processes. Consequently, based on the results of the dilatometry experiments it is possible to argue that the boron causes a delay in the bulk transport processes responsible for the shrinkage of the powder compact. It is important to note that the pre-sinter of the dilatometer samples with and without boron addition were carried out in a single furnace run and no temperature difference between the samples is expected since they were positioned very

close to each other. Thus it is possible to attribute the delay in the shrinkage to the presence of boron.

Another interesting characteristic of the samples with boron addition is the fact that the linear shrinkage rate progressively increases between 722 °C and 820 °C. Above this temperature, the linear shrinkage rate decreases until approximately 1050 °C is reached. This phenomenon can be related to the formation of TiB particles. Divinski et al. [27] investigated the tracer diffusion of boron in pure α-Ti by secondary ion mass spectroscopy using the stable ^{11}B isotope. They observed that at temperatures below 760 °C, diffusion profiles of acceptable quality could no longer be measured, probably due to the low solubility of boron in α-Ti. Furthermore, they reported that boron is the fastest diffuser in α-Ti after hydrogen. It is important to note that for the formation of TiB particles, a solid state diffusion process needs to take place between boron from amorphous boron powder and titanium from the Ti-6Al-4V alloy powder. Therefore, it is reasonable to assume that TiB particles could be formed above 820 °C. As mentioned above it is well known [1-3] that TiB particles can restrict grain growth in cast Ti-6Al-4V alloys. By extension of this concept, it can also be assumed that the initial and intermediate sintering stage (the sintering process, as described by German [26], can be divided into three stages: initial, intermediate and final) can be inhibited by the presence of TiB particles as well.

The Ti-6Al-4V alloy exhibited a maximum linear shrinkage rate of 0.25 %/min at approximately 985 °C. Above this temperature the linear shrinkage rate started to decrease which is an indication of the initiation of the final sintering stage. For most

materials, it is common that separation of grain boundaries and pores occurs, leaving the pores isolated in the grain interior at the final sintering stage [28]. This leads to coarsening of the microstructure and further elimination of the porosity (further densification) becomes difficult since lattice diffusion is needed, which is much slower than grain boundary diffusion.

On the other hand, the Ti-6Al-4V-0.5B alloy starts to shrink significantly above 1050 °C. The maximum linear shrinkage rate achieved for this alloy during dilatometry experiments was approximately 0.45 %/min at around 1250 °C. It is important to note that the maximum linear shrinkage rate for Ti-6Al-4V-0.5B was approximately two times higher than for the alloy without boron. This behaviour can be explained in terms of the densification and coarsening processes. As pointed out before, the presence of TiB particles restricts grain growth. Consequently, at higher temperatures, the separation of pores and grain boundaries might be delayed. This leads to an optimum configuration for the elimination of pores by grain boundary diffusion. Such behaviour has been reported by Zovas and German [29] for sintered molybdenum. They showed that silica dispersoids retard molybdenum grain growth and consequently higher densification was achieved.

In fact, the addition of boron to a Ti-6Al-4V alloy results in a delay of the bulk transport processes responsible for the shrinkage of the powder compact. Most probably due to the formation of TiB particles, the shrinkage process is retarded from 820 °C up to 1050 °C. This delay in densification occurred due to the pinning effect promoted by the presence of TiB particles. However, such a pinning effect is beneficial to densification

in the later stages of the sintering process as the separation of pores and grain boundaries is postponed which extends the time scale for the elimination of the pores by grain boundary diffusion.

4.3. Tensile properties

As reported in the literature [6, 30], TiB particles tend to reduce the ductility of the Ti-6Al-4V alloy. Such behaviour was also observed for the Ti-6Al-4V-0.5B samples produced by MIM (Table 3). However, the level of this expected reduction was rather moderate (~ 2 %).

As can be seen in Table 2, impurity levels for the samples with and without boron are almost the same. As reported in [31], a certain variation in the interstitial element contents is expected for the samples processed by MIM even if high process quality is assured. In addition, according to that study the measured variation cannot explain the differences in tensile properties. In fact, the presence of TiB particles in the titanium matrix is assumed to be the main reason for the significant increase in strength and the decrease in ductility. In this study, the ductility was quantified in terms of tensile elongation to failure. Sen et al. [6] studied the influence of small additions of boron in cast Ti-6Al-4V alloys on the tensile properties. They observed that the tensile elongation to failure shows a maximum at a level of 0.05 wt. % boron and that further additions of boron promoted embrittlement of the alloy. The possible reason for the degradation in the ductility at higher concentrations of boron (the maximum amount of boron they investigated was 0.4 wt. % and the corresponding tensile elongation to failure was 5.2 %) was related to the brittle TiB particles that decorate the grain boundaries. Such preferential precipitation of the TiB particles apparently does not

occur in the MIM Ti-6Al-4V-0.5B alloy, which is a clear advantage of the MIM process over the casting process. It is important to note that even with 2 % residual porosity and with 0.5 wt. % of boron, the tensile elongation to failure of the MIM Ti-6Al-4V-0.5B alloy was ~ 12 % which is much higher than the values obtained by Sen et al. for a cast alloy. In addition, in that study the average grain size reached was larger than 100 µm even for the alloy with 0.4 wt. % boron.

The white arrows in Fig. 7 indicate broken TiB particles and interfacial decohesion between TiB particle and the matrix. Moreover, fine and coarse dimples with residual porosity were typical features of the tensile fracture surfaces. The existence of dimples, being a typical feature of the ductile fracture of metallic materials, is in agreement with the relatively high values obtained for the tensile elongation to failure.

4.4. Fatigue behaviour

The fatigue behaviour of Ti-6Al-4V alloy fabricated by MIM technology has been discussed in previous publications [11, 15] in terms of the fracture surface and the fatigue crack nucleation mechanisms. In these investigations, the authors assumed that crack nucleation is related to dislocation pile-ups, leading to the formation of quasi-cleavage facets on the possible crack nucleation region of the fracture surface. Another typical microstructural feature of the crack nucleation region was the presence of pores. As can been seen in Fig. 10, these quasi-cleavage facets and pores were also observed at the possible crack nucleation locations in Ti-6Al-4V-0.5B. It is important to note that the apparent nucleation site is located inside the sample instead of on the surface. Internal fatigue origin is frequently encountered in titanium alloys after shot peening

[32-34] mainly due to the introduction of compressive surface stresses. Such a phenomenon was observed in all fracture surfaces of the Ti-6Al-4V-0.5B alloy.

As pointed out by the white arrows in Fig. 10a, interfacial decohesion (pull-out) between TiB particles and matrix may had occurred during the crack initiation in MIM Ti-6Al-4V-0.5B. Soboyejo et al. [35] proposed that the pull-out of TiB particles is a relevant fatigue crack nucleation mechanism in order to explain the fatigue results obtained for an ingot of a Ti-6Al-4V-0.5B alloy.

As described before, the boron addition induces a refinement of the microstructure. It is well known that refinement of the microstructure can promote an increase in the fatigue strength of Ti-6Al-4V, from 440 to 670 MPa as reported in [36]. Furthermore, the TiB particles are expected to effectively decrease the slip length when compared to the slip length of a fully lamellar Ti-6Al-4V alloy [2, 37, 38]. Therefore, the reduction in the slip length, which means a more homogeneous distribution of dislocation density, is assumed to be the main origin of the significant enhancement of the fatigue behaviour by adding boron as observed in this work.

Flat surfaces which are an indication of quasi-cleavage fracture and micro cracks are typical features of the crack front profile near the assumed crack nucleation site (Fig. 11 and Fig. 12). The micro cracks exhibited microscopic deflection, which is a well known mechanism in the crack propagation behaviour of $\alpha + \beta$ titanium alloys with a lamellar microstructure [21]. Furthermore, micro cracks are apparently formed near TiB particles, which is a further indication of the interfacial decohesion between the matrix

and the TiB particles as clearly illustrated in Fig. 12b. Most probably, such a phenomenon is associated with stress concentrations promoted by the particles and due to the dislocation pile-ups at the particles.

As a result, for nearly fully dense materials, it is possible to assume that a fine microstructure can tolerate a higher number of defects than a coarse microstructure. Such an assumption has already been proposed in a previous paper by Ferri et al. [16]. In their study, they observed that the negative influence of porosity on the fatigue life was more than compensated for by the finer microstructure (smaller slip length). It is also important to note that apart from the typical crack nucleation mechanisms in the Ti-6Al-4V alloy fabricated by MIM technology, a further mechanism, the interfacial decohesion between matrix and TiB particles, apparently occurs during crack nucleation in the Ti-6Al-4V-0.5B alloy. However, even with a possible additional mechanism for the crack nucleation process, the high cycle fatigue behaviour of the boron containing alloy was superior to that of the alloy without the boron addition.

4. Summary

In the present work, the effect of a small boron addition to the Ti-6Al-4V alloy was investigated in terms of microstructural evolution and the sintering behaviour. The addition of 0.5 wt. % boron leads to a significant refinement of the microstructure. This refinement is mainly due to the fact that TiB particles act both as new nucleation sites for the α phase (heterogeneous nucleation) and as pinning sites to restrict grain growth. The Ti-6Al-4V-0.5B alloy exhibits a microstructure with α colonies (lamellar structure)

and α grains (equiaxed structure) instead of the typically fully lamellar microstructure obtained in the Ti-6Al-4V alloy produced by the MIM process.

Although the addition of boron results in a delay of the sintering process, the final density is increased. Furthermore, the TiB particles exert a pinning effect on grain growth. This serves to postpone the separation of pores and grain boundaries and is thus beneficial for densification in the later stages of sintering.

Significant increases in yield stress and UTS were observed for the alloy with the boron addition. However, as a consequence of the presence of TiB ceramic particles, the ductility decreased compared to the alloy without boron addition. The Ti-6Al-4V-0.5B alloy processed by MIM achieved an endurance limit of ~ 640 MPa which is a significant improvement compared to the alloy without the boron addition (~ 450 MPa). Similar crack nucleation features are observed in both alloys. These common features were the quasi-cleavage facet, which is formed due to dislocation pile-ups, and the presence of pores at the assumed crack nucleation location. Apart from these features, a further mechanism may have occurred during the crack nucleation process in the alloy with boron: interfacial decohesion between matrix and TiB particles.

The refinement of the microstructure due to the presence of boron provides a simple possibility to fabricate titanium-based alloys by MIM technology with tensile and fatigue behaviour in the range of annealed, wrought Ti-6Al-4V alloys.

5. Acknowledgements

The authors would like to express their gratitude to Dr. P. Beaven and Dr. S. Yi for their assistance in the acquisition and interpretation of the EBSD results. For the helpful discussions along the manuscript preparation, Dr. N. Hort and Prof. Dr. M. Dahms are gratefully acknowledged.

References

[1] I. Sen, U. Ramamurty, "Mechanical behaviour of B modified Ti-6Al-4V alloys", presented at *Ti-2007 Science and Technology*, **2007**.

[2] W. Chen, C. J. Boehlert, *Materials Science and Engineering A* **2008**, *494*, 132.

[3] M.J. Bermingham, S.D. McDonald, K. Nogita, D.H.ST. John, M. S. Dargusch, *Scripta Materialia* **2008**, *59*, 538.

[4] S. Tamirisakandala, R.B. Baht, J.S. Tiley, D.B. Miracle, *Scripta Materialia* **2005**, *53*, 1421.

[5] D.B. Miracle, R. Srinivasan, J. S. Gunasekera, *Advanced Materials & Processes, December* **2006**, 41.

[6] I. Sen, S. Tamirisakandala, D.B. Miracle, U. Ramamurty, *Acta Materialia* **2007**, 4983.

[7] Y. Komizo, H. Terasaki, M. Ikeda, F. Nishino, M. Toudai, "Fine-grained titanium by inclusion-assisted microstructure control ", presented at *Ti-2007 Science and Technology*, **2007**.

[8] S.C. Tjong, Z.Y. Ma, *Materials Science Engineering* **2000**, *R29*, 49.

[9] H. Ye, X.Y. Liu, H. Hong, *Journal of Materials Processing Technology* **2008**, *200*, 12.

[10] Y. Itoh, T. Harikou, K. Sato, H. Miura, "Improvement of ductility for injection moulding Ti-6Al-4V alloy", presented at *PM2004*, Wien, **2004**.

[11] O.M. Ferri, T. Ebel, R. Bormann, "Fatigue property of Ti-6Al-4V components fabricated by metal injection moulding", presented at *EURO PM2008*, Manheim, **2008**.

[12] M. Niinomi, T. Akahori, M. Nakai, K. Ohnaka, Y. Itoh, K. Sato, T. Ozawa, "Mechanical properties of $\alpha + \beta$ type titanium alloys fabricated by metal injection molding with targetting biomedical applications", presented at *TMS*, **2007**.

[13] J. O. Peters, R. O. Ritchie, *International Journal of Fatigue* **2001**, *23*, 413.

[14] M. Niinomi, *International Journal of Fatigue* **2007**, *29*, 992.

[15] O.M. Ferri, T. Ebel, R. Bormann, *Materials Science and Engineering A* **2009**, *504*, 107.

[16] O.M. Ferri, T. Ebel, R. Bormann, *Material Science and Engineering A* **2010**, *527*, 1800.

[17] S.S. Sahay, K.S. Ravichandran, R. Atri, *Journal of Material Research* **1999**, *14*, 4214.

[18] R. M. German, *Sintering Theory and Practice*, John Wiley & Sons, New York **1996**.

[19] D. Hill, R. Banerjee, D. Huber, J. Tiley, H. L. Fraser, *Scripta Materialia* **2005**, 387.

[20] H. Feng, Y. Zhou, D. Jia, Q. Meng, *Material Science and Engineering* **2005**, *A390*, 344.

[21] X. Zhang, W. Lü, D. Zhang, R. Wu, *Scripta Materialia* **1999**, *41*, 39.

[22] Z.Y. Ma, S.C. Tjong, L. Gen, *Scripta Materialia* **2000**, *42*, 367.

[23] G. Wen, S.B. Li, B.S. Zhang, Z. X. Guo, *Acta Materialia* **2001**, *49*, 1463.

[24] S. Tamirisakandala, R.B. Bhat, V.A. Ravi, D. B. Miracle, *Journal of Metals* **2004**, 60.

[25] R. Srinivasan, D. Miracle, S. Tamirisakandal, *Materials Science and Engineering A* **2008**, *487*, 541.

[26] R. M. German, *Powder Metallurgy Science*, MPIF, Princeton **1984**.

[27] S.V. Divinski, F. Hisker, T. Wilger, M. Friesel, C. Herzig, *Intermetallics* **2008**, *16*, 148.

[28] J. S. Reed, *Principles of Ceramics Processing*, John Wiley & Sons, New York **1995**.

[29] P. E. Zovas, R. M. German, *Metallurgical Transactions A* **1984**, *15*, 1103.

[30] T.M.T. Godfrey, A. Wisbey, P.S. Goodwin, K. Bagnall, C. M. Ward-Colse, *Materials Science and Engineering A* **2000**, *282*, 240.
[31] G.C. Obasi, O.M. Ferri, T. Ebel, R. Bormann, *Material Science and Engineering A* **2010**, *527*, 3929.
[32] M.Y.P. Costa, H.J.C. Voorwald, W.L. Pigatin, V.A. Guimaraes, M. O. H. Cioffi, *Materials Research* **2006**, *9*, 107.
[33] S.A. Namjoshi, V.K. Jain, S. Mall, *Engineering Material and Technology* **2002**, *124*, 222.
[34] X.P. Jiang, C.S. Man, M.J. Shepard, T. Zhai, *Materials Science and Engineering A* **2007**, *468-470*, 137.
[35] W.O. Soboyejo, W. Shen, T. S. Srivatsan, *Mechanics of Materials* **2004**, *36*, 141.
[36] C.A. Stubbington, A. W. Bowen, *Journal of Material Science* **1974**, *9*, 941.
[37] W. Chen, C. J. Boehlert, E. A. Payzant, J. Y. Howe, *International Journal of Fatigue* **2010**, *32*, 627.
[38] C.J. Boehlert, S. Tamirisakandala, D. Miracle, "The effect of boron on the elevated-temperature creep behaviour of cast Ti-6Al-4V (wt.%)", presented at *Ti-2007 Science and Technology*, **2007**.

Tables

Phase	Structure/space group	Unit cell [10^{-10} m]	Atomic positions
TiB	Orthorhombic/Panma	a = 6.12 b = 3.06 c = 4.56	Ti: 4c, m, x = 0.1777, y = 1/4, z = 0.123 B: 4c, m, x = 0.029, y = 1/4, z = 0.603
TiB_2	Hexagonal/P6/mmm	a = 3.03 c = 3.23	Ti: 1a, 6/mmm, x = 0, y = 0, z = 0 B: 2d, $\bar{6}$ m2, x = 1/3, y = 2/3, z = 1/2

Table 1 – Crystal structure, lattice parameters and fractional coordinates in TiB and TiB_2 [17].

Material	O [µg/g]	C [µg/g]	N [µg/g]
Ti-6Al-4V-0.5B	1960 ± 21	390 ± 33	164 ± 6
Ti-6Al-4V[15]	1917 ± 30	450 ± 13	180 ± 9

Table 2 – Chemical concentrations of interstitial elements.

Material	$\sigma_{0.2}$ [MPa]	UTS [MPa]	Plastic Elongation [%]
Ti-6Al-4V-0.5B	787 ± 1	902 ± 2	11.8 ± 2
Ti-6Al-4V[15]	703 ± 6	806 ± 3	13.7 ± 1

Table 3 – Tensile properties of MIM Ti-6Al-4V with and without boron.

Figures

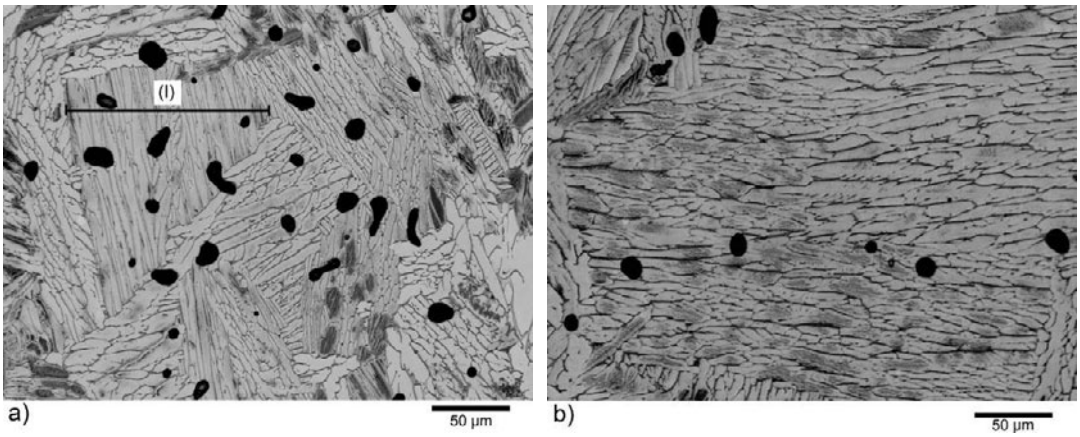

Fig. 1. Light microscopy images of the microstructure of Ti-6Al-4V samples sintered at: a) 1250 °C, and b) 1400°C. A typical lamellar structure is observed with residual porosity. The length (I) represents an α colony size.

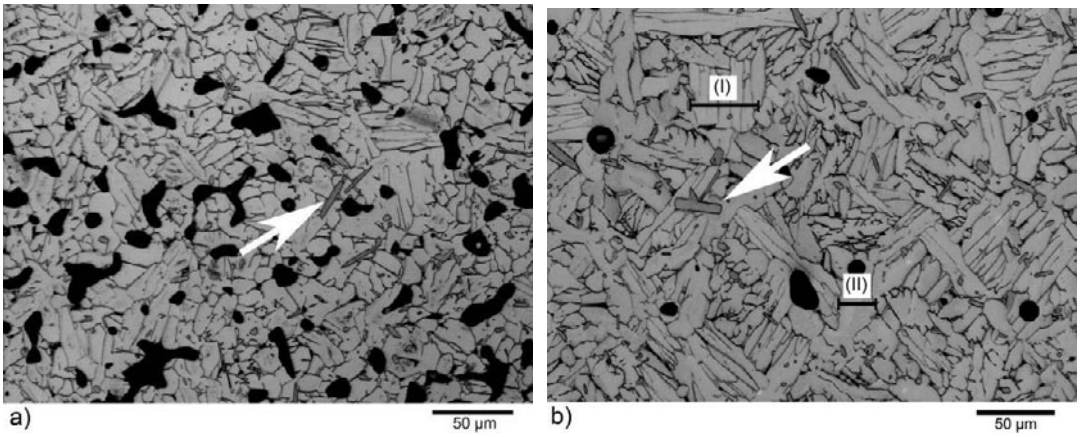

Fig. 2. Light microscopy images of the microstructure of Ti-6Al-4V-0.5B samples sintered at: a) 1250 °C and b) 1400 °C. The large black regions are pores and the white arrows indicate the borides in form of needles. Length (I) represents the size of an α colony and the length (II) illustrates the size of a single α grain.

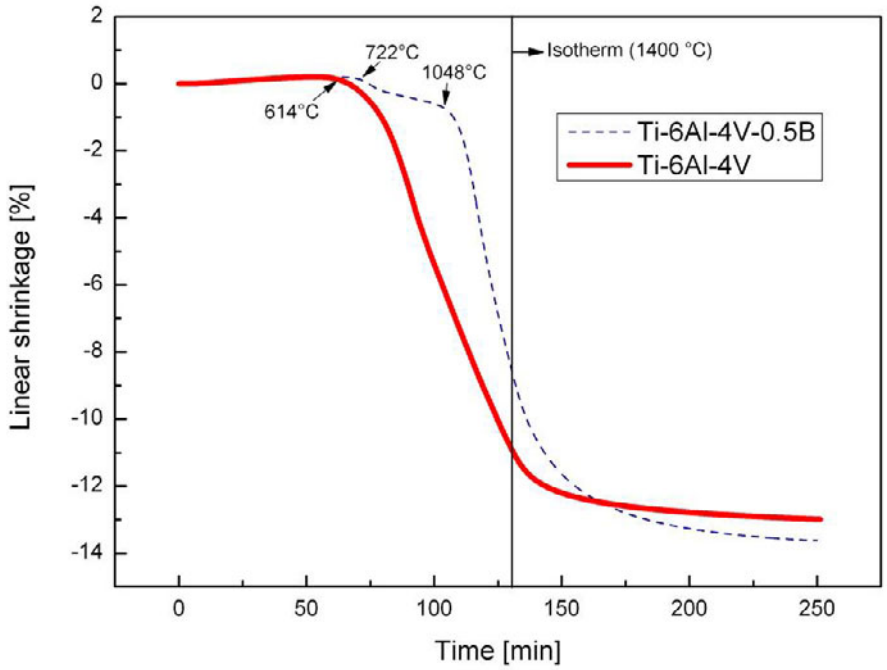

a)

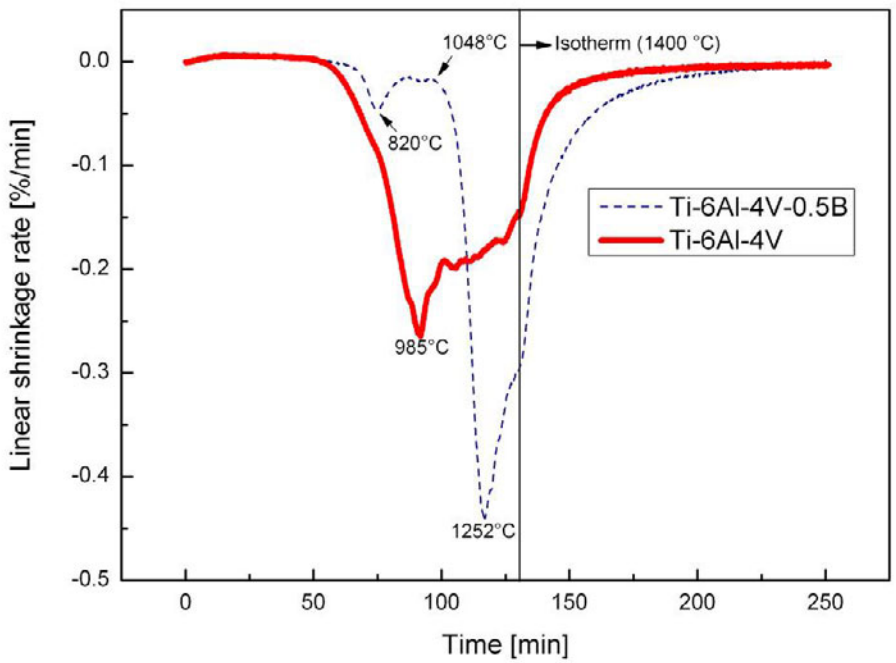

b)

Fig. 3. Dilatometry of Ti-6Al-4V and Ti-6Al-4V-0.5B alloys: a) linear shrinkage (LS) and b) linear shrinkage rate (LSR). Acquisition of data started at 75 °C.

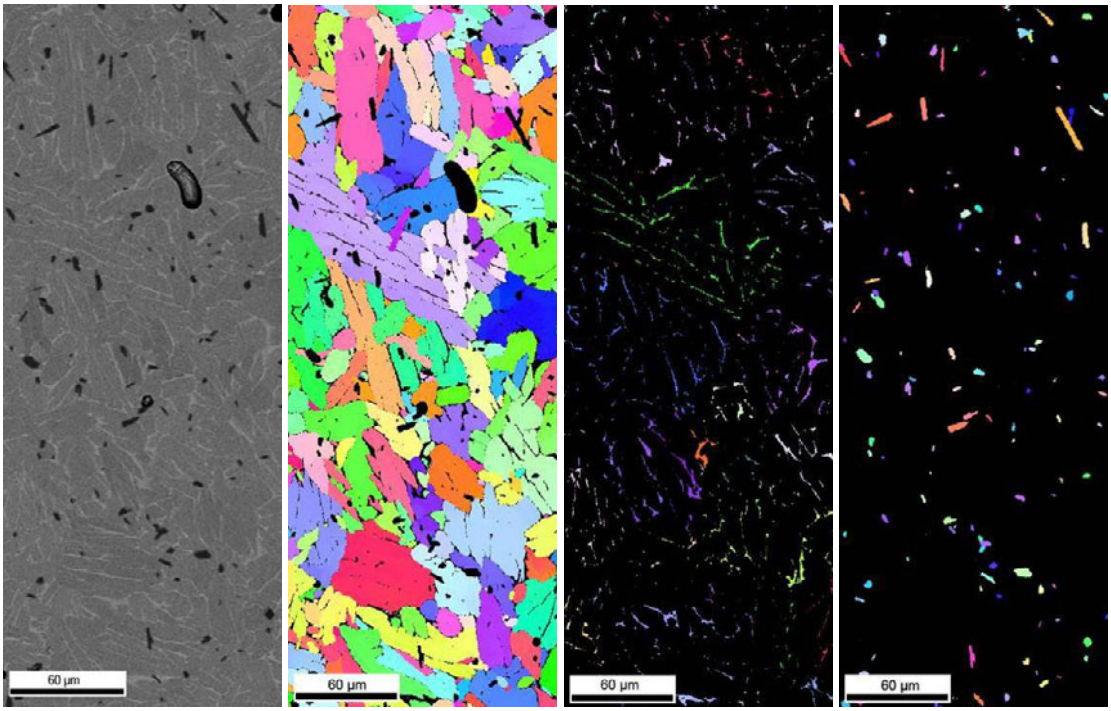

a) b) c) d)

Fig. 4. EBSD phase map of Ti-6Al-4V-0.5B sintered at 1400 °C: (a) BSE image, (b) α phase, (c) β phase and (d) TiB particles. Each colour (grey scale for copy) is related to a specific orientation.

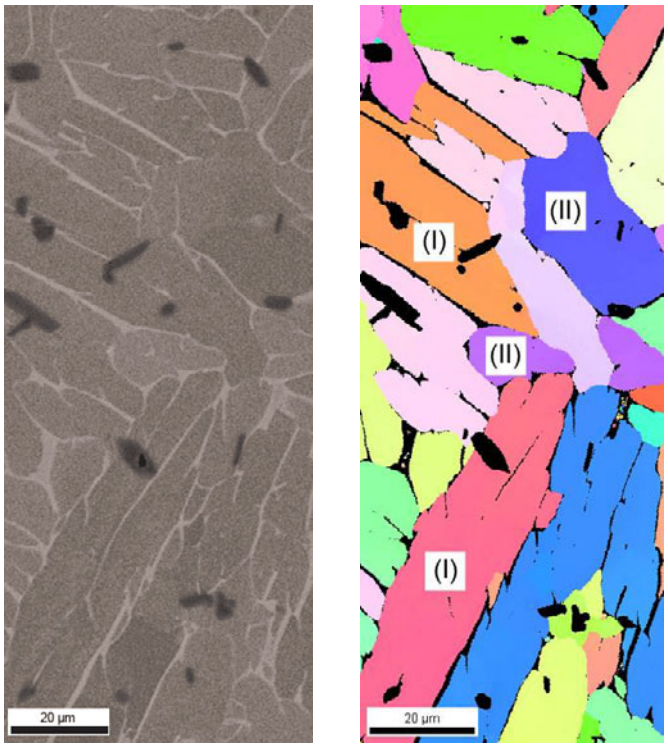

a) b)

Fig. 5. High magnification EBSD phase map of Ti-6Al-4V-0.5B sintered at 1400 °C. (a) BSE image, (b) α phase.

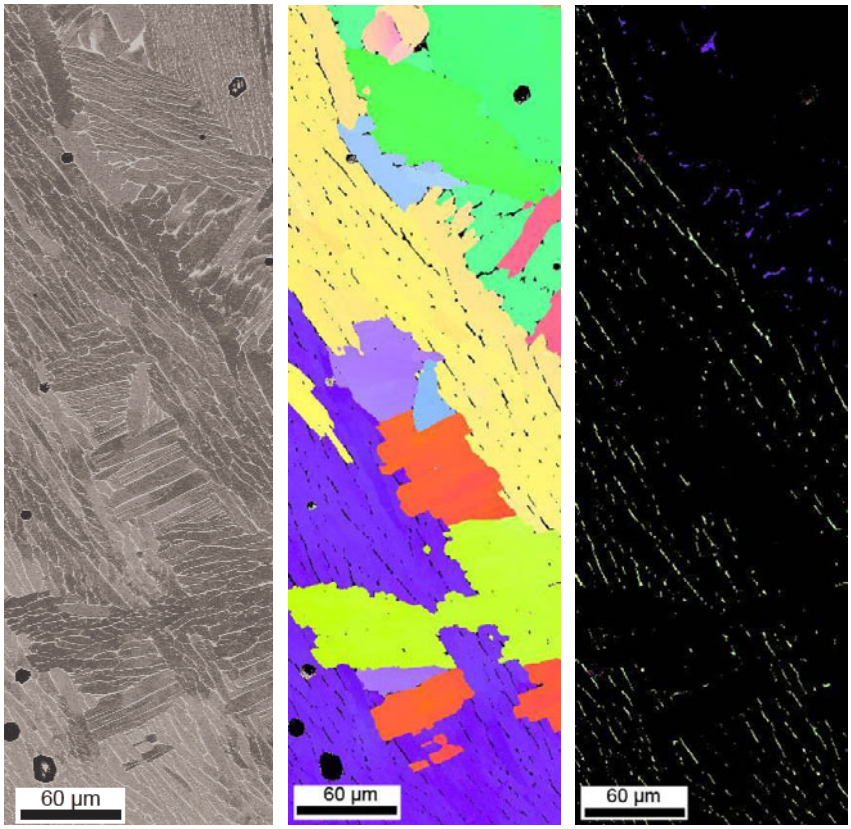

a) b) c)

Fig. 6. EBSD phase map of Ti-6Al-4V sintered at 1400 °C: (a) BSE image, (b) α phase and (c) β phase. Each colour (grey scale for copy) is related to a specific orientation.

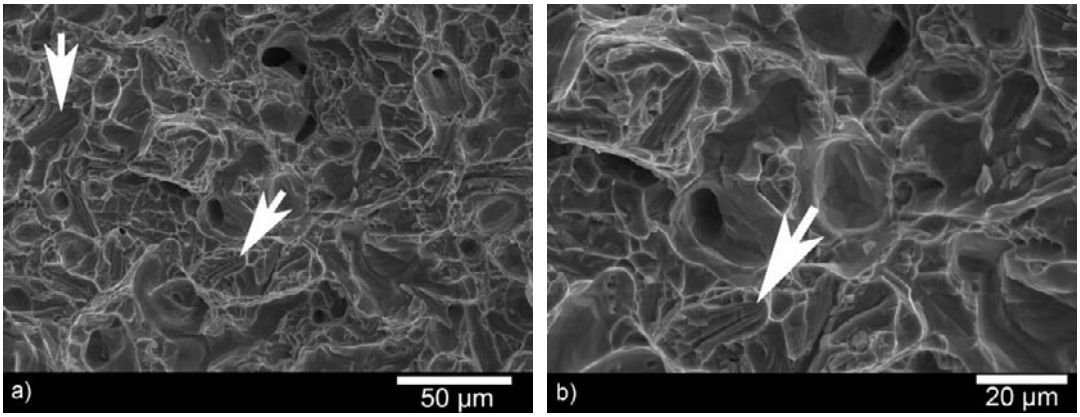

Fig. 7. Typical tensile fracture surface of Ti-6Al-4V-0.5B processed by MIM. Fine and coarse dimpled structures and pores are visible. Additionally, broken and debound TiB particles are indicated by the white arrows.

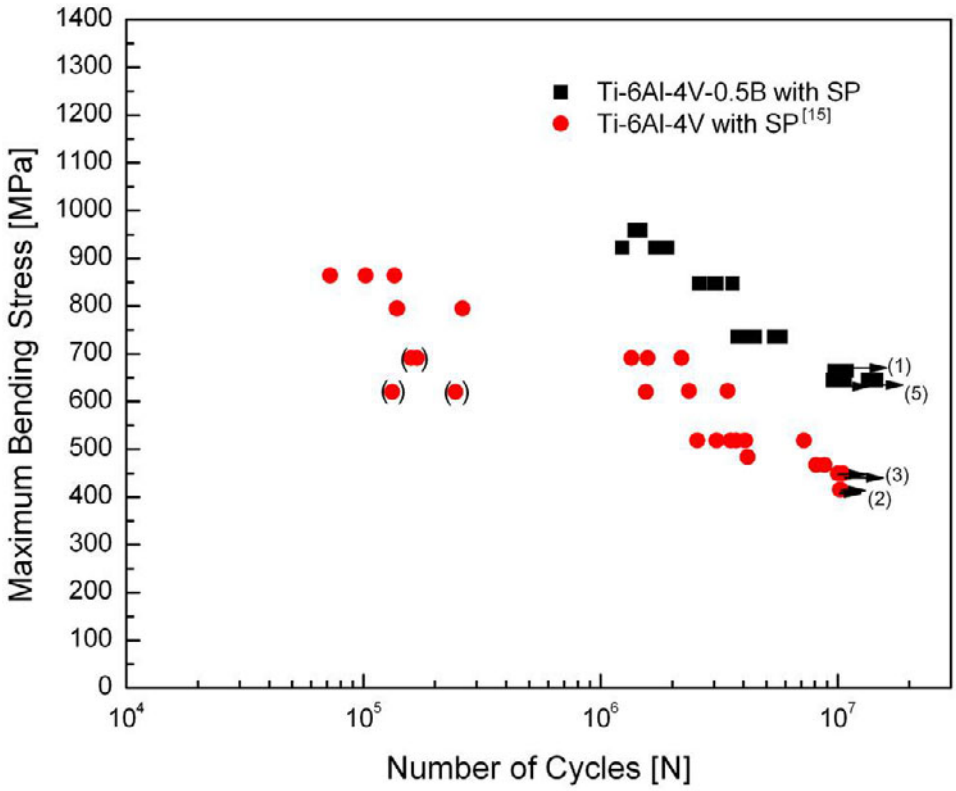

Fig. 8. S-N curves of Ti-6Al-4V and Ti-6Al-4V-0.5B alloys with shot peening (SP). The numbers between parentheses indicate the number of samples that survived at a specific stress level (run out).

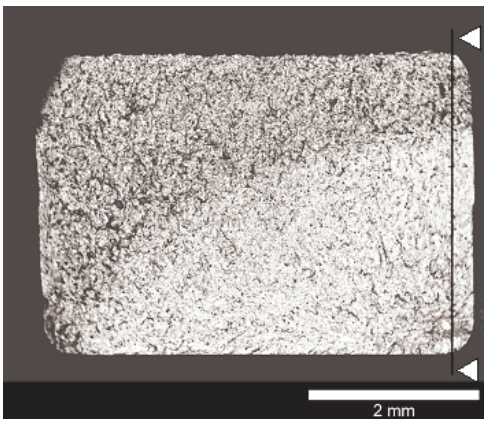

Fig. 9 – Typical BSE micrograph of the fracture surface of a Ti-6Al-4V-0.5B sample sintered at 1400 °C. The black line indicates the approximate position where the crack front profile (Fig. 11) was evaluated.

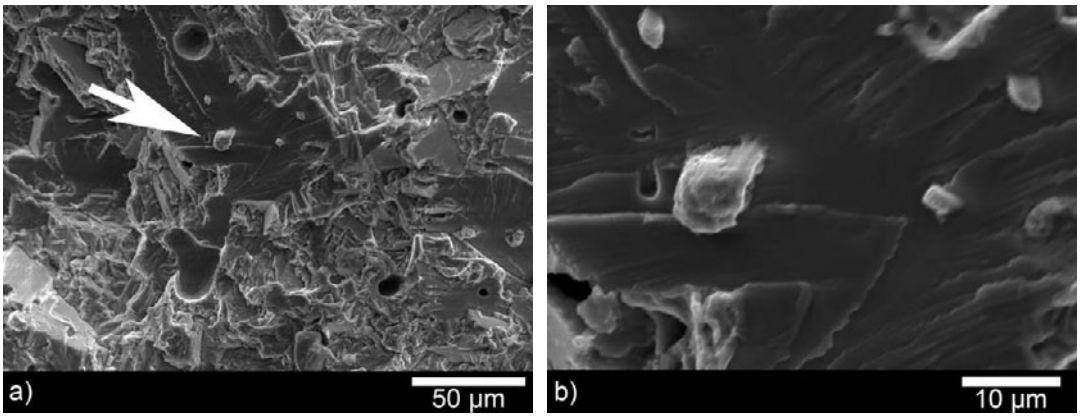

Fig. 10. Typical SE micrograph of the fracture surface of a Ti-6Al-4V-0.5B sample sintered at 1400 °C.

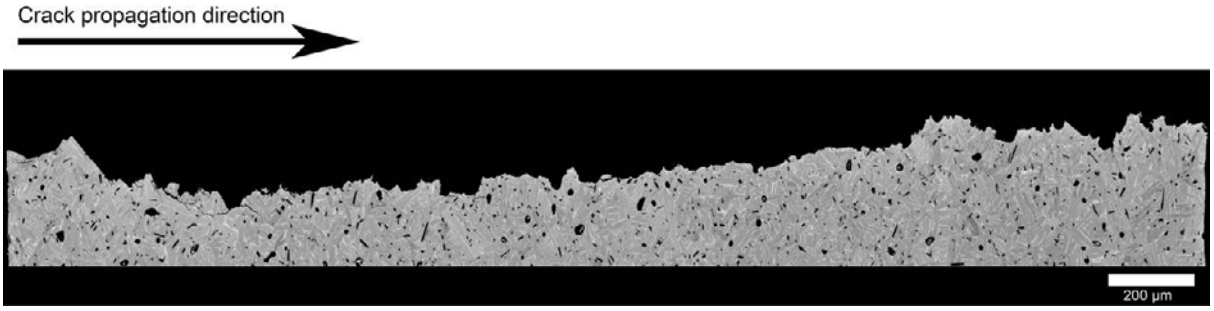

Fig. 11 – Typical crack front profile of a Ti-6Al-4V-0.5B sample sintered at 1400 °C. The investigated region is pointed out in Fig. 9.

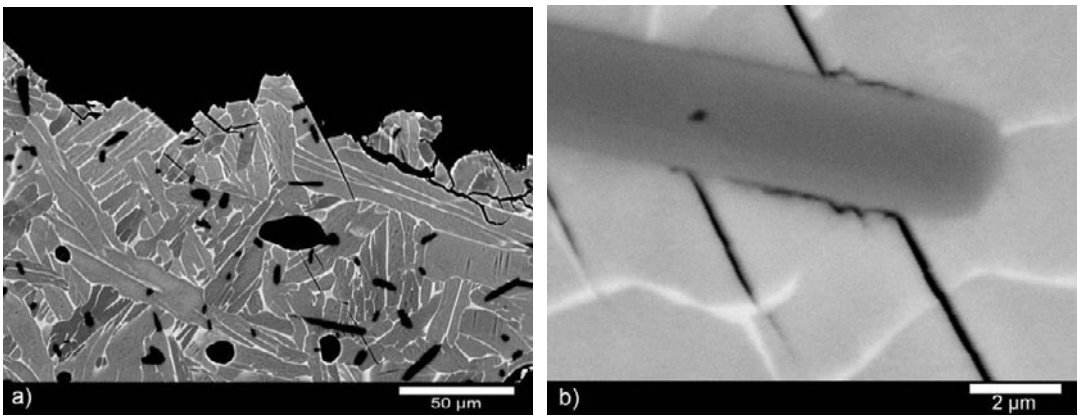

Fig. 12 – Higher magnification of the crack front profile of a Ti-6Al-4V-0.5B sample sintered at 1400 °C: (a) at crack nucleation site and (b) the interaction between a secondary crack and the TiB particle.